Materials Science and Engineering C 59 (2016) 565–576

Contents lists available at ScienceDirect

Materials Science and Engineering C

journal homepage: www.elsevier.com/locate/msec

Characterization, corrosion behavior, cellular response and *in vivo* bone tissue compatibility of titanium–niobium alloy with low Young's modulus

Yanjie Bai [a,b,1], Yi Deng [a,c,1], Yunfei Zheng [a], Yongliang Li [a], Ranran Zhang [d], Yalin Lv [d], Qiang Zhao [b,*], Shicheng Wei [a,c,*]

[a] Department of Oral and Maxillofacial Surgery, Laboratory of Interdisciplinary Studies, School and Hospital of Stomatology, Peking University, Beijing 100081, China
[b] Department of Stomatology, Aviation General Hospital of China Medical University and Beijing Institute of Translational Medicine, Chinese Academy of Science, Beijing 100012, China
[c] Center for Biomedical Materials and Tissue Engineering, Academy for Advanced Interdisciplinary Studies, Peking University, Beijing 100871, China
[d] Department of Stomatology, Beijing Anzhen Hospital, Capital Medical University, Beijing 100029, China

ARTICLE INFO

Article history:
Received 9 June 2015
Received in revised form 2 October 2015
Accepted 20 October 2015
Available online 21 October 2015

Keywords:
β-Type titanium
Titanium–niobium alloy
Low Young's modulus
Biocompatibility
Bone tissue compatibility

ABSTRACT

β-Type titanium alloys with a low elastic modulus are a potential strategy to enhance bone remodeling and to mitigate the concern over the risks of osteanabrosis and bone resorption caused by stress shielding, when used to substitute irreversibly impaired hard tissue. Hence, in this study, a Ti–45Nb alloy with low Young's modulus and high strength was developed, and microstructure, mechanical properties, corrosion behaviors, cytocompatibility and *in vivo* osteo-compatibility of the alloy were systematically investigated for the first time. The results of mechanical tests showed that Young's modulus of the Ti–Nb alloy was reduced to about 64.3 GPa (close to human cortical bone) accompanied with higher tensile strength and hardness compared with those of pure Ti. Importantly, the Ti–Nb alloy exhibited superior corrosion resistance to Ti in different solutions including SBF, MAS and FAAS (MAS containing NaF) media. In addition, the Ti–Nb alloy produced no deleterious effect to L929 and MG-63 cells, and cells performed excellent cell attachment onto Ti–Nb surface, indicating a good *in vitro* cytocompatibility. *In vivo* evaluations indicated that Ti–Nb had comparable bone tissue compatibility to Ti determined from micro-CT and histological evaluations. The Ti–Nb alloy with an elasticity close to human bone, thus, could be suitable for orthopedic/dental applications.

1. Introduction

Compared with other traditional metallic biomaterials, such as Co–Cr alloys and stainless steels, titanium (Ti) and its alloys have become the most attractive metallic materials used in medical applications, especially in orthopedic and dental implants, owing to their combined advantages of high strength-to-weight ratio, excellent corrosion resistance, and favorable biocompatibility [1,2]. These attractive performances promote the development and application of new orthopedic Ti alloys in the medical area. The first generation orthopedic α + β titanium alloys like Ti–6Al–4V is being widely employed and has received good clinical outcomes. The Ti–6Al–4V alloy has cornered almost all of the market for cementless total hip arthroplasties because it has good specific strength in comparison to pure Ti [3,4]. However, the elastic modulus of Ti–6Al–4V alloy (110 GPa) is still much greater than that of human cortical bone (10–30 GPa) [1,5]. The large elastic modulus mismatch between implants and surrounding bone tissue has been identified as a major cause of pain when walking, stress shielding, implant loosening, and even bone resorption [6,7]. And the moduli mismatch could lead to excessive micro-motion between implants and bone, which prohibits bone formation and contrarily facilitates fibrous tissue ingrowth, thereby impeding the osseointegration of implant [8]. Moreover, as reported in many previous research and clinical cases, the long-term performance of Ti–6Al–4V alloys also raises great concerns due to the release of Al and V ions, which is harmful to cells and tissues [9–11]. Therefore, a novel Ti-based implant with low elastic modulus and high strength for bone tissue engineering is much-needed.

With developing of material science and technology, the second generation β-type Ti-alloys with lower Young's moduli have been invented for orthopedic application to resolve these adverse effects of Ti–6Al–4V alloy on bone. Ti–Ni alloy once was considered as implantable material over last two decades, because of its unique shape-memory effect, super-elasticity and high damping [12,13]. The release and accumulation of Ni ions, nevertheless, are thought to be a potential risk, which may be toxic to human body, influence gene expression and cholesterol metabolism, and cause allergy/carcinogenicity. Thus, Ni-free β Ti-alloys have been widely studied. Recently, a large number of new β-type binary Ti alloys have been developed *via* the addition of alloying

* Corresponding author.
E-mail addresses: 15911025865@139.com (Q. Zhao), sc-wei@pku.edu.cn (S. Wei).
[1] These authors contributed equally to this study.

http://dx.doi.org/10.1016/j.msec.2015.10.062
0928-4931/

elements such as Mo, Nb, Ta, Zr and Hf to suppress the elastic modulus and enhance the strength of Ti alloys. On the other hand, some research on the biological behavior of metals have shown that the composition of metallic implant must be carefully selected to avoid or minimize adverse reactions [14,15]. Among these binary Ti alloys, therefore, the Ti–Nb alloy has drawn considerable attraction for its great potential as implant material in orthopedic and dental applications owing to its non-toxic, good biocompatibility and superb corrosion resistance [16–18]. Similar to Ti, Nb is highly unreactive and biocompatible in the body. Previous literature pronounces that Nb element is good for the osteogenesis in animal implantation tests [19,20], and favorable for cell adhesion, proliferation and differentiation *in vitro* studies [21, 22]. Although there are some research focusing on the mechanical properties and corrosion behavior of Ti–45Nb previously, to our knowledge, little work has been probed regarding *in vitro* cell responses and *in vivo* bone tissue compatibility of the Ti–45Nb binary alloy. Hence, in the present study, the microstructure, mechanical properties, electrochemical performances, *in vitro* biocompatibility and *in vivo* osteocompatibility of the Ti–Nb alloy with the pure Ti as a control group were systematically investigated as the critical step towards its use for biomedical applications. Compared with bare Ti, the Ti–Nb alloy could effectively reduce Young's modulus to close to human cortical bone, and promote the corrosion resistance capability of Ti. Simultaneously, Ti–Nb alloy implant possessed comparable *in vitro* cytotoxicity, *in vivo* osseointegration and bone formation with the commercial Ti, presenting a bona fide potential as implant material for orthopedic/dental applications.

2. Materials and methods

2.1. Alloy preparation

Sponge titanium (ASTM grade 2) and niobium ingots were used as primary materials, all chemically 99.9% in purity. The Ti–Nb ingots were prepared by arc-melting on a water-cooled copper hearth under an argon inert atmosphere with a nonconsumable tungsten electrode. A vacuum of 5×10^{-4} was created before argon injection. The ingots were turned around and re-melted five times for homogeneity, and hot rolled into rods. The rods were then heat treated in a vacuum atmosphere at 1123 K for 1 h followed by water quenching. Finally, disc samples with 8 mm in diameter and 1 mm in thickness were prepared for material characterization and *in vitro* testing, and screw-shaped samples with 10 mm in length and 4 mm in diameter were designed for *in vivo* bone compatibility studies. Samples of the alloy were polished with a series of increasing SiC abrasive papers (400, 800, 1500, 2000 grit) and burnished with colloidal silica to give a mirror-like finish. Then, they were cleaned ultrasonically for 30 min in baths of acetone, anhydrous ethanol, and de-ionized water (D.I. water), respectively, and dried at 50 °C overnight. The commercial pure Ti (grade 2, purchased from Northwest Institute for Non-ferrous Metal Research, China) was used as a control throughout the study due to its excellent biocompatibility and it was one of the major metals used in dental/orthopedic implants.

2.2. Surface characterization

The surface chemical constitution and elemental state of the prepared samples were characterized by energy dispersive spectrometry (EDS, EDAX, USA), auger electron spectroscopy (AES, PHI-700, ULVAC-PHI, Japan), and X-ray photoelectron spectroscopy (XPS, AXIS Ultra, Kratos Analytical Ltd.). Phase characterization was carried out using X-ray diffraction (XRD, DMAX-2400, Rigaku, Japan, monochromatized Cu Kα radiation, $\lambda = 0.15406$ nm, 40 kV, 30 mA). Optical microscopy was taken for microstructure analysis (BX51M, Olympus, Japan) after the Ti–Nb alloy was etched using a solution of 10% HF, 15% HNO_3 and 75% H_2O for 15 s. Atomic force microscopy (AFM, PI3800/SPA400, Seiko Instruments, Japan) using a Si_3N_4 cantilever with a spring constant of 0.12 N/m (Seiko) for resolution imaging was employed in dry condition to assess morphological characteristics of the Ti–Nb alloy substrate in contact mode. Before AFM measurement, the Ti–Nb and bare Ti substrates were rinsed with ethanol and D.I. water, and allowed to air dry. Static contact angles on Ti–Nb surfaces were measured at room temperature by the sessile drop method using 2 μL D.I. water droplet in a contact angle measuring device (SL200B, Kono, USA). Six samples in each stage were used to provide an average and standard deviation.

2.3. Tensile and microhardness tests

The tensile properties (including the yield strength, tensile strength, and Young's modulus) of the Ti–Nb alloy were measured using a materials testing machine (5969, Instron, MA, USA) at a crosshead speed of 0.2 mm/min per ASTM D790. For each group, six duplicate specimens were tested. The fracture morphology of Ti–Nb after uniaxial tensile was further observed by a field emission scanning electron microscope (FE-SEM, JSM-6701F, JEOL, Japan). Hardness of the Ti–Nb alloy was determined by a digital Vickers microhardness tester (HMV-2 T, Shimadzu, Japan) with a 1.96 N load and 10 s dwell time. Six points were chosen and measured in different positions of each sample to get an average value.

2.4. Corrosion behavior tests

2.4.1. Electrochemical measurements

The corrosion behaviors of the Ti–Nb binary alloy and pure Ti were tested in three electrolytes including simulated body fluid (SBF, pH = 7.4), modified Fusayama–Meyer artificial saliva (MAS, pH = 5.0), and fluoridated acidified artificial saliva (FAAS, MAS containing 0.2% NaF and 0.3% lactic acid, pH = 4.0) solutions prepared as described previously [23,24]. The anti-corrosive activities of the pure Ti and Ti–Nb alloy were evaluated by open circuit potential (OCP)-time measurements, electrochemical impedance analysis, and anodic polarization experiments. The electrochemical properties of the studied material surfaces were measured in a glass electrochemical cell at 37 ± 0.1 °C which was connected to a computer-controlled potentiostat (CHI 650C, Chenhua, Shanghai, China). Corrosion tests were performed using the standard 3-electrode cell method [saturated HgCl as the reference electrode, Pt as the counter-electrode, and the exposed surface (1.77 cm^2) of the Ti–Nb and Ti samples as the working electrode]. The OCP of each specimen was continuously monitored for 2 h in electrolytes. Electrochemical impedance spectroscopy (EIS) at the open-circuit potential was carried out with an AC amplitude range of −10 mV to 10 mV and evaluated in the frequency range from 10^{-2} Hz to 10^5 Hz. The EIS data were interpreted in Bode amplitude and phase angle plots using ZSimpWin program. After EIS test, the potentiodynamic polarization measurement was performed with a scan rate of 1 $mV \cdot s^{-1}$. Corrosion parameters including corrosion potential (E_{corr}) and corrosion current density (I_{corr}) can be estimated from the polarization curves by Tafel analysis based on the polarization plots. Three parallel samples were applied for each group in the experiments.

2.4.2. Morphological and chemical characterization of corrosive surfaces

After the electrochemical measurements, surface topographies of the studied materials in the different test solutions were characterized by SEM (JEOL, Japan). XPS (AXIS Ultra) was employed to determine these corrosive surface elemental components and their chemical states. The binding energies were also calibrated by the C 1 s hydrocarbon peak at about 285 eV through the CasaXPS software package.

2.5. Cell culture

Mouse L929 fibroblasts cells and human osteoblast-like MG-63 cells (Cell Bank of Shanghai Institutes for Biological Sciences, Chinese

Academy of Science) were cultured in Dulbecco's modified eagle's medium (DMEM, Gibco, Carlsbad, CA) containing 10% fetal calf serum (Gibco), 100 g/mL streptomycin (Amresco, Cleveland, USA) and 100 g/mL penicillin (Amresco) at 37 °C in a humidified atmosphere of 5% CO_2. The culture media was changed at 2–3 day intervals. Prior to *in vitro* testing, the all samples were sterilized using gamma radiation at a total dose of 25 kg.

2.6. In vitro cytocompatibility evaluations

2.6.1. Indirect cytotoxicity on extracts

Test on extracts was carried out according to the instruction of ISO 10993-5: 2009 in the study. The extraction media of the Ti–Nb alloy and pure Ti specimen were prepared using serum free cell culture medium (DMEM), with the extraction ratio (the ratio of specimen surface area to extraction medium) of 3 cm^2/mL, and then incubated in a humidified atmosphere with 5% CO_2 at 37 °C for 72 h. Cell culture medium (DMEM) was used as a negative control. Cells were incubated in 96-well cell culture plates (Corning, USA) at 5×10^3 cells per 100 μL in each well and incubated for 24 h to allow attachment. Then culture media were substituted by the extracts obtained from the studied materials and incubated for 1, 4, and 7 days, respectively. After the culturing period, the cell viability was measured by reacting with 100 μL/well MTT reagent (Sigma-Aldrich, final concentration 0.5 mg/mL) for 4 h at 37 °C before the addition of 100 μL solubilization solution (10% SDS in 0.01 M HCl). After overnight solubilization, then 100 μL of supernatant from each well was transferred to new 96-well cell culture plates. Optical density (OD value) of the supernatant was measured with a microplate reader (Model 680, Bio-Rad, CA) at 570 nm with the reference wavelength at 630 nm. Six parallel measurements were used to provide an average and standard deviation. The cell viability was expressed as a percentage as following:

$$\text{Cell viability } (\%) = (\text{OD}_{(\text{test})} - \text{OD}_{(\text{blank})}) \,/\, (\text{OD}_{(\text{negative control})} - \text{OD}_{(\text{blank})}) \times 100\%.$$

2.6.2. Direct cytotoxicity on samples

After cell counting, MG-63 and L929 cells were exposed to the Ti–Nb alloy and bare Ti substrates in 24-well plates at a density of 1×10^4 cells/well, respectively. The pure DMEM medium without studied materials was as the negative control. After incubating for 1, 4, and 7 days, respectively, the culture media were removed and the specimen were rinsed with PBS buffered three times in order to remove the unattached cells. Cell viability of the adherent cells was measured by the same MTT approach as the aforementioned description.

2.6.3. Morphology observation of cells

The morphologies of L929 and MG-63 cells co-cultured on Ti–Nb alloy were observed using the FE-SEM after 2 days of culture. All samples were washed with PBS buffer, fixed in 2.5% glutaraldehyde solution for 30 min and then dehydrated with graded ethanol solutions (25%, 50%, 75%, 95%, and 100%, 15 min each concentration). Dehydrated samples were dried by a vacuum dryer before sputter-coating with gold using a sputter coater.

2.7. Alkaline phosphate activity assay

Alkaline phosphatase (ALP) activity of MG-63 cells was evaluated by an assay reagent kit (Nanjing Jiancheng Bioengineering Institute, China). MG-63 cells were exposed to the Ti–Nb and pure Ti samples for 7–21 days, and the pure DMEM medium without studied materials was as the negative control. Briefly, the supernatant was removed and 100 μL of lysis solution (1% TritonX-100) was added into each well and incubated for 1 h. Afterwards, 30 μL of MG-63 cell lysates at each well was transferred to new 96-well cell culture plates, and cultivated with 50 μL of carbonated buffer solution (pH 10) and 50 μL of substrate solution (4-amino-antipyrine) at 37 °C for 15 min. Then 150 μL of potassium ferricyanide was added into the above solution, and the production of *p*-nitrophenol was determined by the absorbance at 405 nm. For normalization, the total protein concentration was measured by a bicinchoninic acid (BCA) protein assay kit (Beijing Biosea Biotechnology, China). Thus, alkaline phosphatase activity was normalized and expressed as the total protein content (μmol/min/μg protein).

2.8. Oral mucosa irritation

Six male New Zealand white rabbits (weight 3–4 kg) were randomly divided into two groups: Ti–Nb alloy and bare Ti. After the rabbits were under general anesthesia (3% pentobarbital sodium, intravenous injection, 1 mL/kg), the Ti–Nb and pure Ti disc samples (5 mm in diameter and 0.5 mm in thickness) were sutured on the maxillary buccal mucosa. The experimental protocol was approved by the Institutional Animal Care and Use Committee of Peking University. After two weeks surgery, the rabbits were euthanized, and the samples discs were removed. The corresponding buccal mucosa tissue contacted with the disc samples were fixed with 4% paraformaldehyde and stained with hematoxylin and eosin (H&E) for histological observation.

2.9. In vivo bone tissue compatibility evaluation

2.9.1. Surgery

Surgical implantation was performed on six female beagle dogs aged 1 year and weighing 10.3–12.9 kg for observation period of 2, 4 and 12 weeks after surgery. The *in vivo* study was conducted according to the ethical principles of the Peking University Institutional Animal Care and Use Committee. All dogs were randomly assigned to two groups corresponding to Ti–Nb alloy and pure Ti control. General anesthesia was achieved using an intravenous injection of 3% pentobarbital 1 mL/kg. Six hole with diameter of 4 mm was prepared at the left and right medial tibia of the beagle using dental drill until the hole reached 7 mm in depth, and the samples were then implanted into the prepared hole. For each group, there were twelve cylindrical implants placed. The dogs received subcutaneous injection of oxytetracycline (30 mg/kg) and ketoprofen (3 mg/kg) for 3 consecutive days. After surgery, two fluorochromes (Sigma), i.e. calcein (50 mg/kg), and tetracycline hydrochloride (50 mg/kg) were administered to assess the osteogenic activity at week 2 and 4, respectively. The dogs were sacrificed at 2, 4 and 12 weeks after surgery by an intracardiac injection of 10% kalium chloratum (0.5 mL/kg).

2.9.2. Micro-CT analysis

High-resolution images of all the specimens after surgery were obtained from a micro-computed tomography scanner (SKYSCAN 1076, Skyscan Company) running at 100 kV, 80 μA and a resolution of 18 μm. A polygonal region of interest (ROI) in 600 slices with approximate 200 μm wide ring around implant surface was chosen, which represented the regenerated bone only. After scanning, the three-dimensional (3D) models were reconstructed from the volume of interest, where an optimized threshold was used to isolate the bone and materials from the background using the NRecon (Skyscan Company) and CTVol (Skyscan Company, Belgium). The percent bone volume (BV/TV) of trabecular bone and cortical bone around the implant was calibrated and determined by the CTAn program (Skyscan Company) after 2, 4, 12 weeks post-operation.

2.9.3. Bone histomorphometric analysis

After micro-CT, the tibia with the implants were harvested and fixed in 10% buffered formalin, and dehydrated by ascending concentrations of ethanol. The samples were embedded in methyl methacrylate resin without decalcification and micron sections were made after polymerization with a microtome (SP1600; Leica, Wetzlar, Germany) along the longitudinal axis of the bone-implant interface. Afterwards, the

embedded tissue samples were cut into sections with a thickness of about 30 μm for fluorescence labeling observation under the confocal laser scanning microscope (CLSM, LSM710 NLO, Zeiss, Oberkochen, Germany) to observe bone integration with the host tissue. The excitation/emission wavelengths used to observe chelating fluorochromes were 405/575 nm and 488/520 nm for tetracycline hydrochloride (yellow) and calcein (green), respectively. Histomorphometric analysis to evaluate the percentages of new bone contact and bone area was also performed on the same sections of each group.

2.10. Statistical analysis

All data were expressed as mean ± standard deviations (SD) of a representative six similar experiments carried out. Statistical analysis was performed by one-way analysis of variance (ANOVA) followed by Tukey's post hoc tests using SPSS 19.0 and *p*-values less than 0.05 were considered statistically significant.

3. Results and discussion

3.1. Chemical composition and microstructural characterization

Results of EDS analysis (Fig. S1(a)) after removing the surface oxide layer showed that the main elements on the surface of the Ti–Nb alloy were Ti and Nb, in which the strongest signal was at 4.5 keV with the second peak at 2.2 keV. The weight percentage of Ti and Nb determined from EDS were 45.87% and 54.13%, respectively. And the chemical composition of Ti–Nb alloy samples determined by AES was mainly consisted of 45.2 wt.% niobium and 54.7 wt.% titanium, similar to the EDS result. To verify the results from EDS and AES, XPS, a surface-sensitive characterization technique, was applied to evaluate the detail chemical bonds formed on the surface of the Ti–Nb alloys. The wide XPS survey spectra and high-resolution Nb and Ti spectra were shown in Fig. S1(b–d). The Ti–Nb alloy displayed strong Ti 2p, Nb 3d, Nb 3p, and O 1s peaks, as well as C 1s. Carbon, typically present from unavoidable hydrocarbon contamination, was used as an internal reference at 284.6 eV for calibrating peak positions [25]. The stoichiometry of Ti/Nb ratio was estimated based on the Ti 2p and Nb 3d spectra data, and the Ti/Nb ratio was about 0.79:1. Moreover, the chemical states of Ti 2p on the surface of Ti–Nb were composed of spin-orbit splitted doublet Ti 2p3/2 at 458.4 eV and Ti 2p1/2 at 464.1 eV, respectively, indicating that TiO_2 was a component in the surface layer of Ti–Nb samples [26]. The binding energies centered around 209.7 and 207 eV were assigned to the Nb-O bond, which coincided with the standard values of Nb_2O_5 [27]. The formation of the oxide was also reflected by the presence of oxygen element. Therefore, it could be concluded that the passive film spontaneously on the Ti–Nb alloy was predominantly composed of TiO_2 and Nb_2O_5. It is reported that the chemical composition and properties of the passive film on the surface have a significant influence on the corrosion behavior and biological performance of metallic materials and implants [28,29].

The surface roughness and wettability of experimental samples were measured and shown in Fig. 1. Top-view surface feature displayed a slightly more rough topography of the Ti–Nb alloy, and the value of average roughness (Ra) varied from 1.63 ± 0.17 μm to 1.79 ± 0.23 μm for pure Ti and Ti–Nb alloy, respectively in a significant way by the area of 100 × 100 μm^2. Water contact angle is a convenient way to assess the hydrophilic-hydrophobic properties of material surfaces. The enhanced hydrophilicity with a lower contact angle (81.75 ± 2.94°) existed for the Ti–Nb alloy compared with that of the bare Ti (96.46 ± 3.56°), and hydrophilic surface is reported to be beneficial to cell attachment and proliferation. The metallographical structure of the Ti–Nb alloy after etching was next shown in Fig. 2 (a–b). The optical micrographs showed that the Ti–Nb alloy had a uniform single β-phase titanium with the grain size of about 10–20 μm. Besides, XRD analysis confirmed the presence of β-type diffraction peak without any α and α" phase in

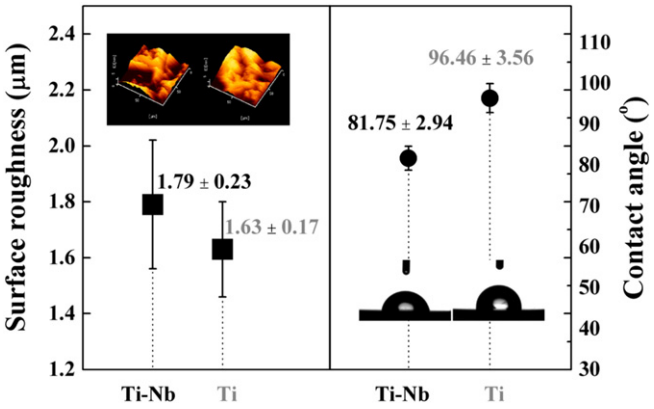

Fig. 1. Surface roughness obtained from AFM images and surface wettability of the Ti–Nb alloy and bare Ti.

the Ti–Nb alloy. Recently, the β-Ti alloys with many advantages comparing to α or (α + β) dual phase Ti-based alloy have raised increasing attention in dental/orthopedic application, such as implants, crowns, and orthodontic wires, due to their much lower elastic modulus, excellent work-hardening, and heat-treatment capabilities [30–33].

3.2. Tensile properties and microhardness of Ti–Nb alloy

The tensile stress–strain curve and mechanical test results of the Ti–Nb alloy were shown in Fig. 3 and Table 1. We could found that the Ti–Nb alloy displayed higher yield strength (438 MPa) and tensile strength (527 MPa), which was about 1.5–1.6 times than those of pure Ti, possibly because the addition of Nb element has a positive role in grain refinement. According to the classic Hall–Petch relationship, the yield strength of the alloy increased with the decrease of grain size [34,35]. Moreover, higher microhardness was detected in the case of Ti–Nb alloy. These indicated that Ti–Nb alloy had better mechanical properties than commercial Ti. However, the Young's modulus of the Ti–Nb binary alloy was decreased to about 64.3 GPa, much closer to human cortical bone (15–30 GPa), and lower than that of commercial Ti (105 GPa, α-type Ti), and other α + β-, and β-type Ti alloys such as Ti–6Al–4 V alloy, 110 GPa; Ti–12Mo–6Zr–2Fe (TMZF), 74–85 GPa; Ti–15Mo–2.8Nb–3Al, 82 GPa; and Ti–29Nb–13Ta–4.6Zr (TNZT), 65 GPa. After introducing the β stabilizing element of Nb into pure Ti, the body-centered cubic (BCC) structure conferred the Ti–Nb alloy with low elastic modulus than the pure Ti with hexagonal close-packed lattice (HCP) [36]. Furthermore, from earlier literature, the results of the theoretical calculation also suggest that Nb element is a suitable alloying element for β-type titanium alloys, capable of enhancing the strength and reducing the modulus of the alloys [35]. As depicted in tensile stress–strain curve (Fig. 3(a)), the Ti–Nb alloy possessed a typical two-stage

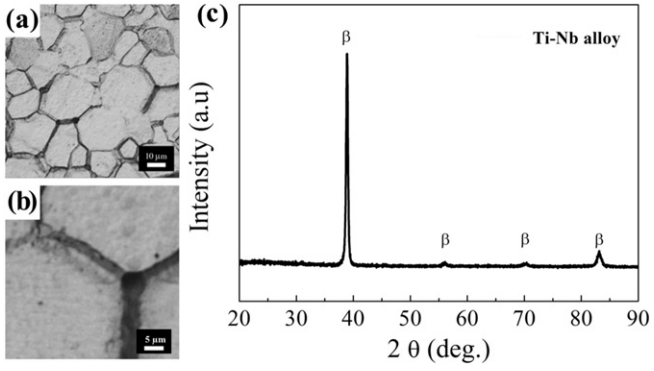

Fig. 2. The metallography (a–b) with different magnifications, and XRD pattern (c) of the Ti–Nb alloy.

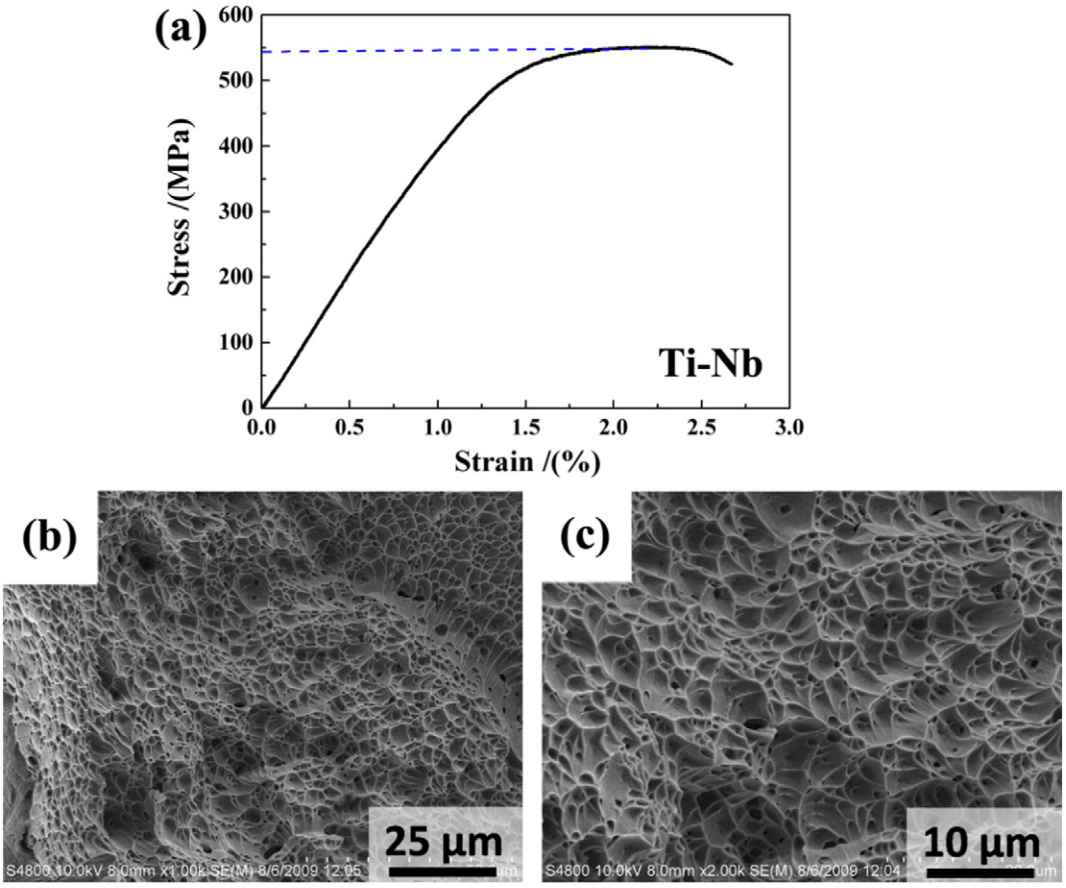

Fig. 3. Stress–strain curves (a) and fracture morphology (b–c) of the Ti–Nb binary alloy.

deformation: elastic deformation before yielding (approximately 438 MPa), and plastic deformation after yielding, besides, it showed a good ductility. The fracture morphology of the Ti–Nb alloy after uniaxial tensile was further observed by SEM. the fracture morphology of tensile specimen was a dimple pattern with the size of 2–4 μm, with an evidence of ductile fracture as shown in Fig. 3(b–c). Commercially pure Ti (α-type) and Ti–6Al–4 V alloy (α + β-type) are commercially available and currently used as biomaterials in orthopedic/dental applications such as bone plates, intramedullary nails and artificial joints because they have excellent corrosion resistance and biocompatibility [37]. Nevertheless, the Young's modulus of these α-type or α + β-type Ti-based alloys is much greater than that of human cortical bone. Hence, the mismatch of the Young's modulus between implants and bone tissue could have a risk of stress shielding, bone resorption and poor osseointegration [6,7]. On the other hand, too low elastic modulus would lead to the micro-motion of metallic implant, resulting in implant loosening, and even failure of prostheses. In general, hence, the Young's modulus of implantable materials should be slightly higher than adjacent bone tissue. In accordance with previous works, a Ti–Nb alloy developed as a β-type Ti alloy with the mechanical properties of low elastic modulus (a bit higher of human cortical bone), good ductility, and high strength/hardness in this work, had a potential use in biomedical area, which mitigated concerns over the risks of osteanabrosis and bone resorption caused by stress shielding.

3.3. Corrosion property of Ti–Nb alloy

3.3.1. Electrochemical corrosion behavior

The corrosion resistance of the Ti–Nb alloy in MAS, SBF, and FAAS was evaluated by open circuit potential (OCP)-time measurements, anodic polarization experiments and electrochemical impedance analysis. Fig. 4(a–b) showed the OCP and potentiodynamic polarization curves of pure Ti and Ti–Nb alloy. OCP is the potential of the working electrode relative to the reference electrode without any applied current, reflecting the thermodynamic equilibrium at the interface of metal and solution as a function of time. As seen in Fig. 4(a), the all OCP curves of Ti–Nb alloy and Ti took on an upward trend and became stable gradually in MAS and SBF solution. However, in FAAS solution, the OCP curves of Ti–Nb alloy as well as pure Ti declined sharply at the initial stage and were then stable at a low potential. In comparison to the

Table 1
Typical tensile test and microhardness value of the Ti–Nb alloy, pure Ti, other β-type Ti alloys, and cortical bone.

	Yield strength (MPa)	Tensile strength (MPa)	Young's modulus (GPa)	Hardness (MPa)
Ti–Nb	438	527	64.3	233.4
Ti–29Nb–13Ta–4.6Zr [55]	368	593	65	200
Ti–15Mo–2.8Nb–3Al [56]	771	812	82	/
Ti–12Mo–6Zr–2Fe [56]	1000–1060	1060–1100	74–85	/
Ti (grade 2) [57]	275	344	105	193.1
Cortical bone [56]	30-70	70-150	15-30	/

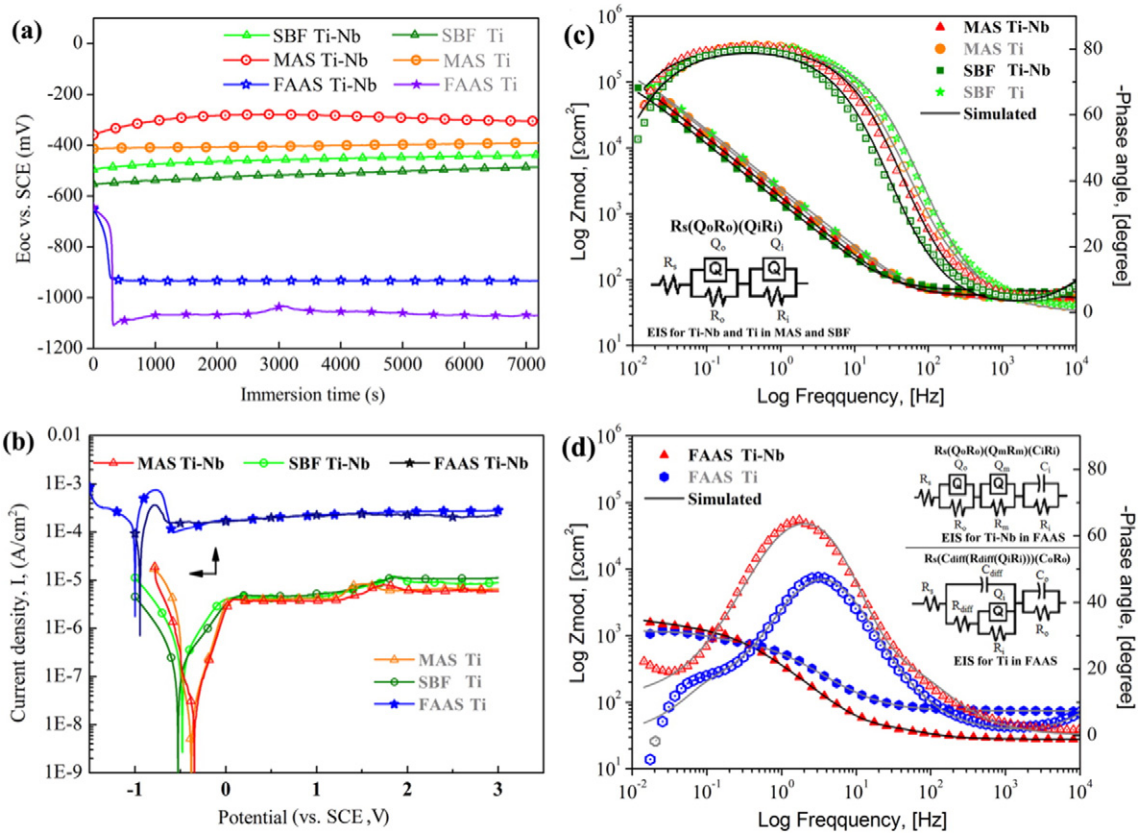

Fig. 4. (a) Open-circuit potential and (b) potentiodynamic polarization curves of the Ti–Nb binary alloy, and pure Ti tested in MAS, SBF and FAAS solutions. Representative EIS diagrams and the equivalent electrical circuit models: (c) fitting result of the Ti–Nb alloy and pure Ti in MAS and SBF solutions; (d) fitting result of the Ti–Nb alloy and pure Ti in FAAS solution.

bare Ti, the OCP-time curves of Ti–Nb specimens shifted upwards (the more noble direction) and reached to the average potentials of −305.0 mV, −439.3 mV, and −933.1 mV after 2 h in MAS, SBF, and FAAS solutions, respectively, which indicated the improved corrosion resistance behavior of Ti–Nb alloy. By comparing the three solutions, the addition of fluoride aggravated the corrosion behaviors of the Ti–Nb alloys and pure Ti seriously with the reduction of OCP values, which suggested fluoride ion had played an important role in corrosion resistance, and pure Ti was easier to be attacked. After 2 h OCP tests, the potentiodynamic polarization curves were also measured in MAS, SBF and FAAS solutions, as shown in Fig. 4(b). The Ti–Nb alloy exhibited polarization behaviors similar to pure Ti and showed broad passivation regions in FAAS solution. Furthermore, consistent with the results of OCP, Ti–Nb alloy samples displayed higher corrosion potential (E_{corr}) and lower corrosion current density (i_{corr}) than those of bare Ti counterpart in all three solutions, as listed in Table 2. While in the fluoridated acidified artificial saliva FAAS (0.2% NaF, pH = 4.0) (Fig. 4(b)), the shape of curves were quite different from that in MAS and SBF solutions (F-free). Potentials displaced towards the negative direction (more than 0.5 V, form −500 mV to −1000 mV) and passive current positioned at a very high place (change from 10^{-5} to 10^{-4} A·cm^2). The Ti–Nb alloy located beneath Ti, which demonstrated the former had a better corrosion resistance than the latter even at extreme conditions with both fluoride and lactic acid. Actually, Nb has a higher standard electrode potential than Ti [38]. In the previous studies, the Ti alloys containing heavy metal elements (such as Nb, Au, Ag, and, Pd) had been proven to exhibit an promoted corrosion resistance [23,39–41]. Due to high corrosion resistance of added noble metals, Ti may dissolve preferentially during the initial stage of corrosion and then the noble element atoms of the alloys surface may accumulate because of Ti loss. As a result, the potential of the alloy became further nobler than the critical potential for passivation of Ti, which improved the corrosion resistance of alloys. These values all indicated that the addition of Nb element to Ti could effectively enhance the corrosion resistance properties of the Ti substrate in both fluoride-free, and fluoridated acidified saliva solutions.

Table 2
Corrosion parameters of the Ti–Nb alloy, and pure Ti obtained from electrochemical measurements in three tested solutions.

Solutions	Samples	OCP (mV)	E_{corr} (mV)	i_{corr} (10^{-8}A/cm^2)	R_p (kΩ·cm^2)
MAS	Ti–Nb	−305.0	−492.2 ± 63	9.48 ± 0.75	274 ± 19.3
	Ti	−391.2	−527.0 ± 73	15.01 ± 1.21	173 ± 0.44
SBF	Ti–Nb	−439.3	−387.9 ± 28	3.93 ± 0.47	659 ± 28.1
	Ti	−485.0	−394.7 ± 24	4.08 ± 1.26	639 ± 28.1
FAAS	Ti–Nb	−933.1	−924.3 ± 41	5261.2 ± 60.8	0.498 ± 0.08
	Ti	−1070.3	−1004.9 ± 72	9980.2 ± 102.5	0.261 ± 0.05

In order to furter study the corrosion resistance of the Ti–Nb alloy, electrochemical impedance spectroscopy (EIS) of the samples at E_{corr} after immersion 2 h in MAS, SBF and fluoride-containing FAAS media were presented, respectively, in the form of Bode-phase and Bode-magnitude plots as depicted in Fig. 4(c–d). It could be observed from Fig. 4(c), profiles of the spectra for Ti–Nb alloy and pure Ti in MAS (F-free, pH = 5.0) and in SBF (F-free, pH = 7.4) were almost overlapped. However, in the FAAS solution (Fig. 4(d)) the phase angle decreased largely at intermediates frequencies, and there was a significant difference in the profiles, indicating changes of the passive oxide films on the surface of Ti–Nb and Ti alloys due to the presence of F^- ions. In the case of pure Ti in the fluoridated acidified solution, the phase angle shifted to −48° higher than that of Ti–Nb (−67°) at intermediates frequencies, and the modulus of impedance at low frequencies dropped even more than Ti–Nb alloy. Besides, the linear slope the spectra was not −1, those meant that the alteration of the passive film of Ti was accelerated by the presence of F ions at a lower pH in this solution.

EIS is a tool used to analyze complex electrochemical systems through evaluation with equivalent circuit modeling, and three equivalent circuit models were proposed here to numerically fit the measured impedance data at different conditions. In the present experiment, the $R_s(Q_oR_o)(Q_iR_i)$ equivalent circuit model based on a two layer structure (an inner compact layer and an outer relatively porous layer) was proposed to fit the EIS data for the two experimentl metals in SBF and MAS solutions. $R_s(Q_oR_o)(Q_mR_m)(C_iR_i)$ model was employed to fit the Ti–Nb alloy in FAAS (0.2% NaF, pH = 4.0), and model $R_s(C_{diff}(R_{diff}(Q_iR_i)))(C_oR_o)$ fit for pure Ti in FAAS. For the $R_s(Q_oR_o)(Q_mR_m)(C_iR_i)$ model, the passive surface of Ti–Nb alloy was supposed to be composed of three layers: an inner compact layer, a middle porous layer and an outer compact layer. With regard to the $R_s(C_{diff}(R_{diff}(Q_iR_i)))(C_oR_o)$ model, boundaries among the passive layers were not clear, which could be attributed to the diffusion of corrosion products. It has been reported by Ibris et al. that the space charge layer and the complex structure of the oxide film formed on the Ti surface in artificial saliva containing fluoride ions [42]. In all models, C_i, and R_i represented the capacitance and resistance of the inner oxide layer; Q_m and R_m represented the capacitance and resistance of the middle oxide layer; Q_{diff} and R_{diff} represented the capacitance and resistance of the intermediate diffusion combination layer; Q_o and R_o represented the capacitance and resistance of the outer oxide layer; R_s represented the solution resistance of the test electrolyte.

The parameter values obtained by the fitting procedure were shown in Tables S1–S3. The circuit displayed a perfect fit for the experimental data with chi-square (χ) values below 10^{-3}. For the double-layer circumstance (Table S1), comparing the capacitances (Q_i and Q_o) and polarization resistances (R_i and R_o) for the Ti–Nb alloy and Ti sample, it could be evidenced that corrosion protection was predominantly induced by the inner barrier layer, as recently reported by Assis et al. [43]. Furthermore, it was clear that the passive film formed on the Ti–Nb alloy became more stable after immersion in SBF and MAS supported by the highter R_i and decreased Q_i values, consistent with OCP and Tafel plots results, indicating the Nb addition greatly increased the corrosion resistance of Ti–Nb alloy. Next, we could see in Tables S2–S3 that both Ti–Nb alloy and Ti samples were susceptible to corrosion in fluoride-containing solution. For the three layers circumstance, it could be concluded that corrosion protection of Ti–Nb alloy in FAAS was predominantly induced by the inner barrier layer, and the corrosion protection of Ti in FAAS was mainly depended on the both inner and outer barrier layer. These electrochemical corrosion results demonstrated that Ti–Nb binary alloy displayed better anti-corrosive perfomance than pure Ti.

3.3.2. Surface characterization of the bio-corrosive Ti–Nb alloy

The typical SEM images of Ti–Nb alloy and Ti samples surfaces after potentiodynamic polarization measurements were presented in Fig. 5. In comparison to their un-polarized samples, Ti–Nb alloy did not show obvious alteration on its surface morphology after polarized in MAS and SBF, whereas the surface scratch of Ti–Nb alloy was dissolved, corrosive micropits occurred, and dissolution became severe in FAS (0.2% NaF, pH = 5.0). Under the identical testing solution, Ti alloy corroded more badly compared with Ti–Nb alloy, especially in fluoride-containing solutions.

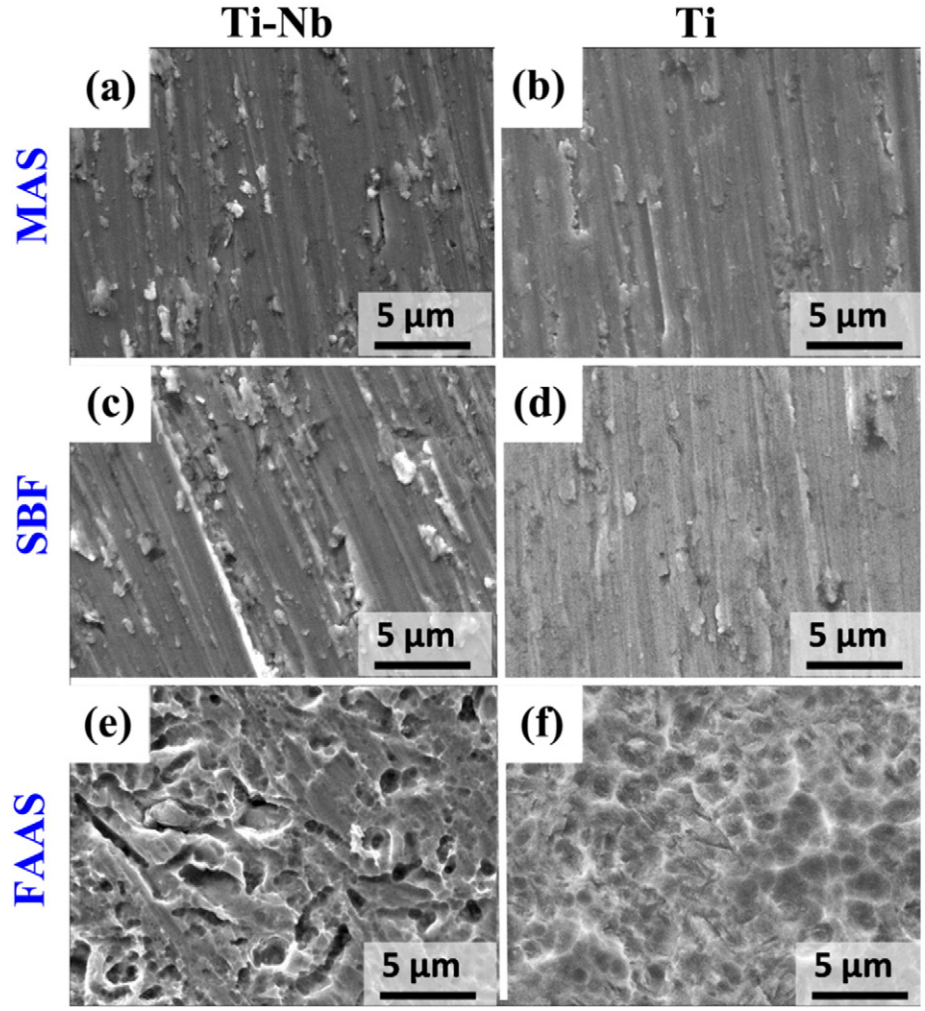

Fig. 5. SEM images of the corroded surfaces of the Ti–Nb alloy (a, c, e) and Ti alloy (b, d, f) in the various solutions.

Fig. S2 showed the XPS wide survey spectra of each tested specimens after the series electrochemical measurements in three solutions. From Fig. S2(a), it revealed that the main chemical composition of the surface layer for Ti–Nb alloy after corrosion tests in all solutions were TiO_2 and Nb_2O_5, while the corrosive surface composition of pure Ti after polarized was mainly constituted by TiO_2. There was little alteration of elements for Ti–Nb alloy in three solutions, however, as for pure Ti, the most noticeable change was the decrease of Ti and O contents, with the increase of C element, resulting from the gradual dissolution of TiO_2 in the presence of F ions. Furthermore, the Nb/Ti ratio increased from 1:5 in MAS to 1:2 in FAAS solution, suggest more dissolution of TiO_2 than Nb_2O_5. Metal and its alloys for orthopedic/dental applications are known to rely on their surface oxides for corrosion resistance, and the passive film had an important effect on corrosion protection of metallic implant [23]. It is proved the protective TiO_2 passive film formed on Ti is vulnerable to fluoride ion [44]. In this study, the increased corrosion resistance of Ti–Nb alloys indicated the addition of Nb helped to form the spontaneous passive film (complex TiO_2 and Nb_2O_5 layer) on the metallic surface which is more stable thermodynamically [23,45], especially in FAAS solution with both fluoride and lactic acid. These results suggested that the Nb_2O_5 layer on the Ti–Nb alloy exert a positive effect on preventing Ti alloy from being attacked by fluoride ions. The SEM and XPS analysis were in accordance with the open circuit potential measurements, electrochemical impedance spectroscopy studies and polarization tests.

3.4. In vitro cytocompatibility

A good biocompatibility with the surrounding tissue cells is usually expected for implantable biomaterials, therefore, the cytocompatibility test of the Ti–Nb alloy regarding of the murine fibroblast cells L929 and human osteoblast-like MG-63 cells was probed in this study. Fig. 6(a) showed the relative viability of two cells cultured in extracts of Ti–Nb alloy for 1, 4 and 7 days, respectively, with bare Ti as control. It could be seen that the cell viabilities of both L929 and MG-63 cells cultured in Ti–Nb alloy extracts were almost the same as those in pure Ti (an average of 93%) within 7 days. The statistical analysis indicated no significant difference between Ti–Nb alloy and pure Ti, representing a non-toxicity feature. The cell proliferation and cytotoxicity of Ti–Nb disc was also evaluated by the MTT assay at from 1 day and 7 days through the direct contact method. After 7 days of culture, the proliferation of L929 and MG-63 cells cultured on Ti–Nb alloy surface varied between 92.1% (Day 14) and 107.3% (Day 4) as shown in Fig. 6(b). Differing from indirect cytotoxicity results, the cell viabilities of MG-63 cells on the Ti–Nb alloy surface were higher than that of pure Ti at Day 4 (Fig. 6(b)). Also no significant differences in cell viabilities of both L929 and MG-63 cells with the results of the TCP plate used as a negative control at each culture period confirmed that Ti–Nb alloy did not induce cytotoxic effect on cells, consistent with previous literature that Ti and Nb element showed an excellent biocompatibility *in vitro*. To further examine the toxicity of Ti–Nb alloy, adherent morphologies of the cells were probed. The typical overview of L929 and MG-63 cells morphologies grown with Ti–Nb alloy and pure Ti specimens for 2 day was illustrated in Fig. 7. It could be seen that cells exhibited extended and polygon-like morphology with many pseudopodium and a cytoplastic shape on the surfaces of Ti and Ti–Nb alloy. Compared with the Ti counterpart, higher amount of cells with better adhesion and spreading was observed in the Ti–Nb group. In addition, good correspondence could be found between the direct observation and the indirect cell viability evaluation. Ti is known to be nontoxic and cytocompatible because a stable oxide film forms on its surface, which shows good biocompatibility, and can effectively inhibit the release of metal ions. Besides, the alloying element Nb also recognized as a biocompatible heavy metal element, and has been used in the applications of orthopedics and medical apparatus [46,47]. In combination with the results of the MTT assay,

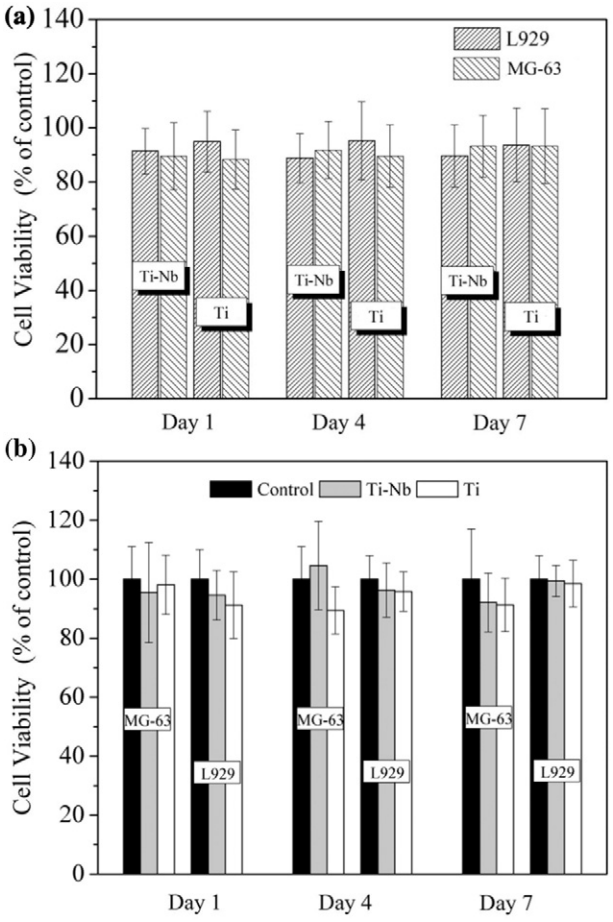

Fig. 6. (a) Indirect cell viability of L929 and MG-63 cells cultured in extracts of the Ti–Nb alloy and pure Ti. (b) Direct cell proliferation of L929 and MG-63 cells cultured on the surfaces of the Ti–Nb alloy and pure Ti.

hence, the conclusion could be drawn that Ti–Nb alloys exerted no negative on the proliferation and growth of cells, thereby showing good *in vitro* cytocompatibility.

3.5. Alkaline phosphatase activity

To successfully apply the Ti–Nb alloy in dental or orthopedic application, favorable osteogenic differentiation activity is needed, usually, the differentiated function of osteoblasts could be evaluated by monitoring alkaline phosphatase (ALP) activity of MG-63 cells. ALP is an important indication of osteoblast cells expressed in their early differentiation phase and a significant quantitative marker of osteogenesis [48]. As depicted in Fig. 8, ALP activity activities increased with time when MG-63 cells were co-cultured with Ti-based materials, indicating that Ti–Nb alloy could induce the ostogenic differentiation of cells. Much higher ALP expression was detected in the case of the Ti-based substrates after 14 and 21 days of growth than the negative control ($p < 0.05$), although no significant differences were detected among groups at 7 days. The enhancement of osteogenic differentiation of Ti–Nb alloy could result from the contacting with the metal surface, because Ti and Nb surfaces were proved to have a positive influence on osteogenesis [19,20,49,50]. However, the statistical analysis indicated that there was no difference between the pure Ti and Ti–Nb alloys for ALP activities of MG-63 cells. It indicated that Ti–Nb alloy had the comparable oseto-differentiation capability of osteoblast to commercial Ti.

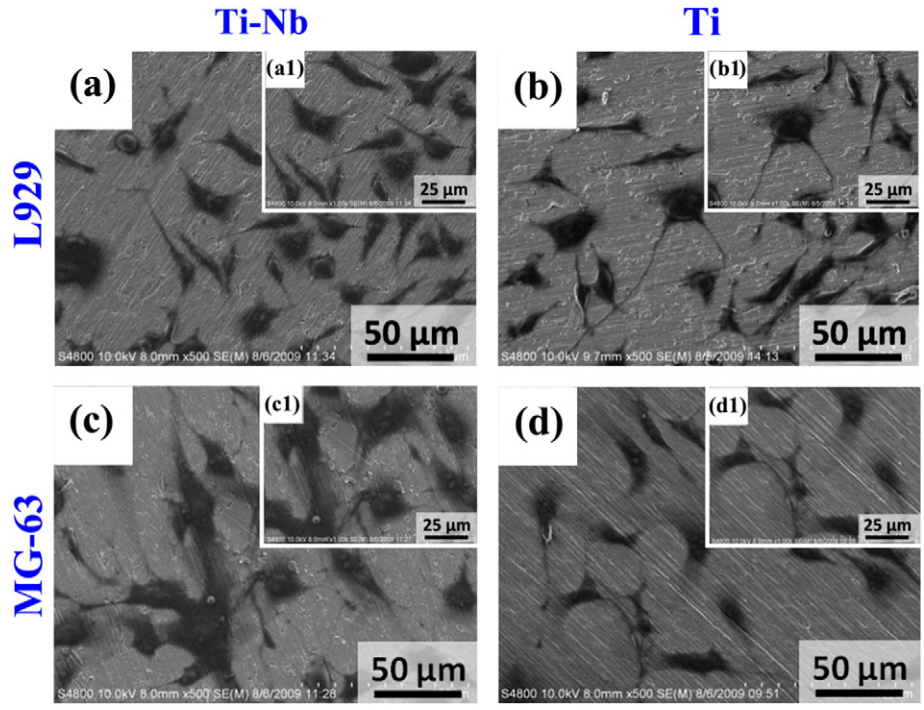

Fig. 7. The cellular morphology of L929 (a–b) and MG-63 cells (c–d) on the Ti–Nb alloy and pure Ti after 2 days of culture.

3.6. Oral mucosa irritation

Next, we performed oral mucosa irritation to determine if Ti–Nb alloy induced inflammatory and allergic reactions in the buccal mucosa. After 14 days, none of the tested parts of New Zealand white rabbits treated with the Ti–Nb alloy and pure Ti alloy displayed erythema or edema reactions. Histological analysis reflected that the buccal mucosa maintained normal epithelium and connective tissue with the absence of inflammatory infiltrate, cellular degeneration and putrescence, engorged blood vessels and no submucous edema with neatly arranged with clear structure as shown in Fig. 9. The two groups showed the same phenomenon after 2 weeks in the cheek pouches of the rabbit, indicating that the Ti–Nb alloy, similar to pure Ti, is not irritant or traumatic to the mucous membranes of mouth. This result confirmed the safety of Ti–Nb to oral mucosa, and Ti–Nb alloy could be used as dental materials in oral environment.

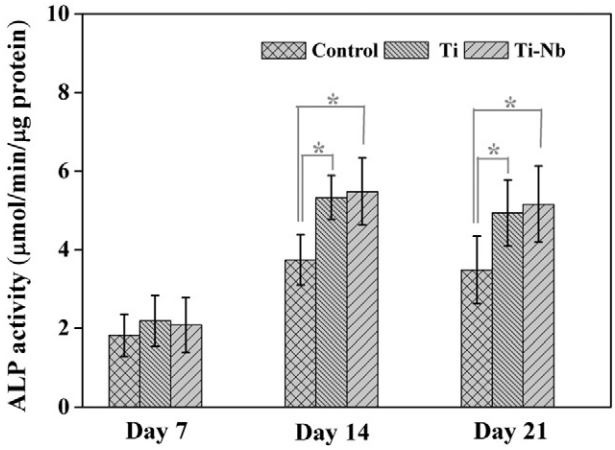

Fig. 8. ALP activity of MG-63 cells after culturing with the Ti–Nb binary alloy and pure Ti for 7, 14, and 21 days. * represents $p < 0.05$ compared with the control group.

3.7. In vivo bone tissue compatibility

3.7.1. Micro-CT

In order to investigate osteo-compatibility, *in vivo* experiments were designed based on our previously established protocol, utilizing a beagle tibia implantation model [51,52]. New bone formation and implant change after operation were evaluated at prescribed time points by micro-CT. The high resolution micro-CT scans in Fig. 10a clearly exhibited continuous parts of the adjacent bone around the implanted Ti–Nb alloy and Ti in the region of trabecular bone and cortical bone area. The implant grooves and threads were also enveloped by new-formed bone, which showed the trabeculae about 0.2 mm thickness vertical to the longitudinal axis of cylindrical implants, indicating that good bone tissue compatibility of Ti–Nb alloy *in vivo*. To assess bone remodeling, the indices of bone histomorphometry from the 3D micro-CT data was further analyzed. Similar peri-implant bone volume/tissue volume (BT/TV) was maintained in both trabecular and cortical bone regions between Ti–Nb alloy and pure Ti implant at 2, 4, and 12 weeks, suggesting that Ti–Nb alloy possessed comparable osseointegration effect to pure Ti, which is widely used as implantable materials in orthopedic/dental applications due to its good bone integration *in vivo*.

In the end, sequential fluorochrome labeling has been used to locate the site of new bone formation since it is designed to bind with calcium ions and to become incorporated into the site of mineralization [53]. The fluorochrome bone marker labels (tetracycline and calcein) were clearly observed for new-formed bone tissue bonding to the cylindrical implants (Fig. 11). All implants showed direct contact with the newly formed bones, and there was no sign of a fibrous layer which implied a loosening of the implants. At 4 weeks, new-formed bone with only green bio-marker could be found in the periphery of all Ti-based implants, while at 12 weeks more double labeling stripes of calcein and tetracycline in appositional new bone was observed under CLSM observation, suggesting the bone deposition and remodeling around the two Ti-based implants. In the dynamic process, the bone contact and bone area of the Ti–Nb alloy rapidly increased up to 12 weeks in all three time points (Fig. S3), with no significant difference with that of Ti, suggesting that the osseointegration of Ti–Nb alloy was as good as Ti.

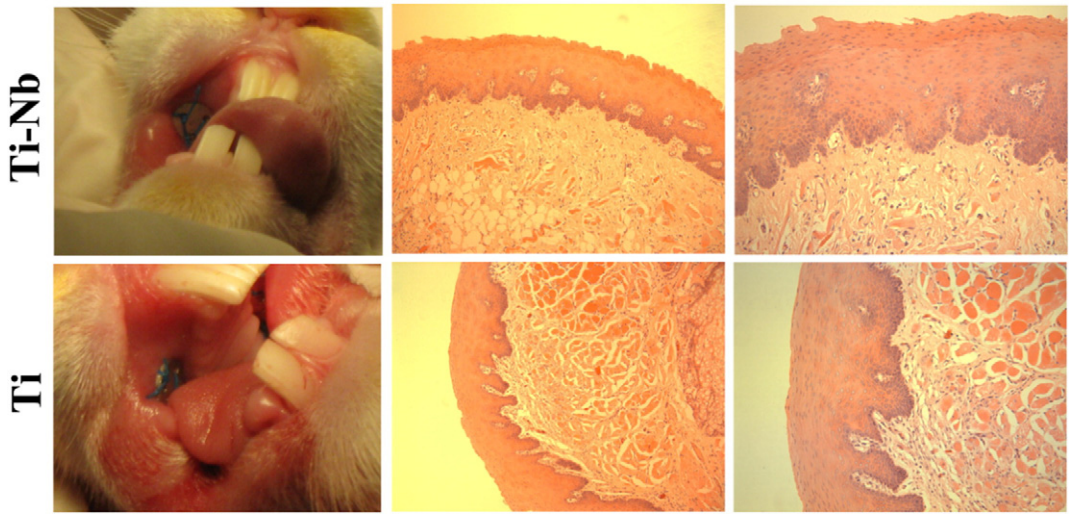

Fig. 9. Photographs of the suture to fix the samples on the cheeks, and histological images of oral irritation reaction of rabbit treated with the Ti–Nb alloy and pure Ti at 12 weeks.

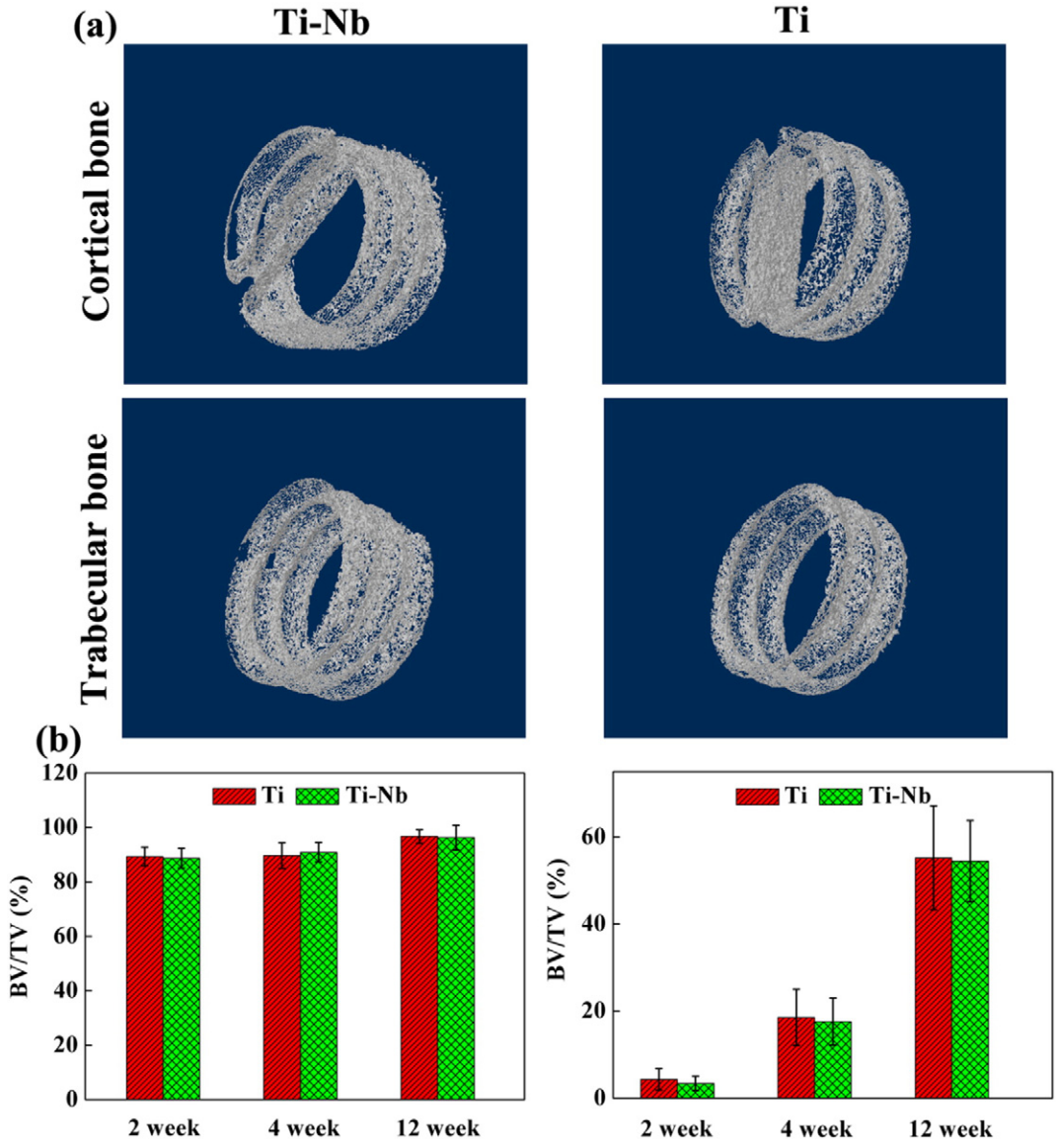

Fig. 10. 3D reconstruction (a) and BV/TV results (b) of trabecular bone and cortical bone for both Ti–Nb and Ti obtained from micro-CT at 12 week.

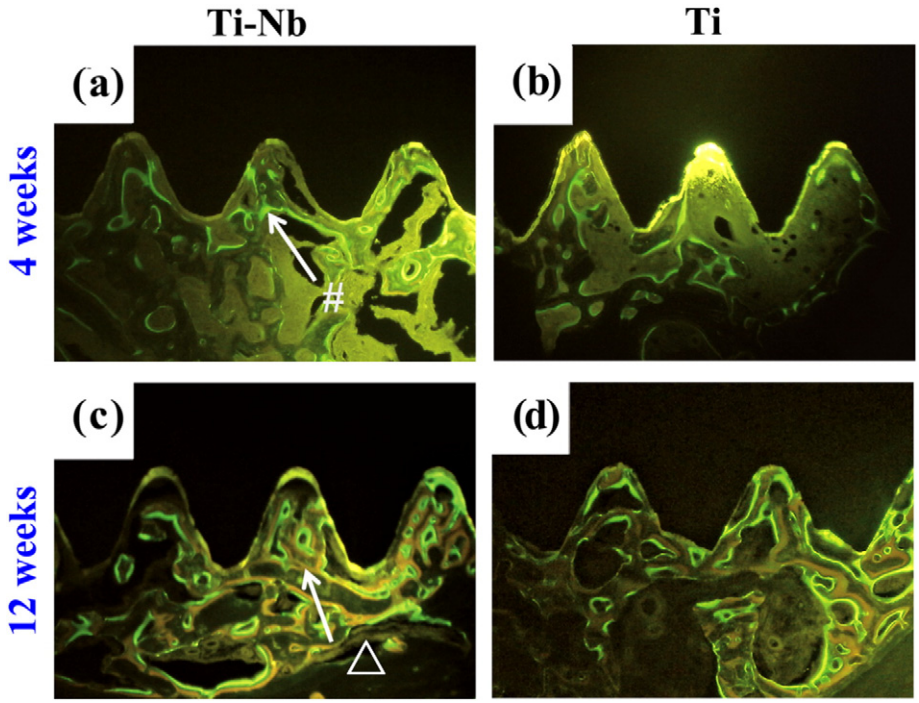

Fig. 11. Histotomy of bone contact of the Ti–Nb alloy (a, c) and Ti (b, d) at 4 weeks and 12 weeks illustrated by fluorescence-dyeing reagents, respectively. Green (#) revealed the new bone formation of 2-week duration dyed by calcein, and the yellow (Δ) revealed that new formation of 4-week duration by tetracycline.

Niinomi et al. evaluated the biocompatibility of a low rigidity Ti–29Nb–13Ta–4.6Zr alloy (Young's modulus 65 GPa) and concluded that the biocompatibility of Ti–29Nb–13Ta–4.6Zr with bone was better than that of stainless steel and Ti–6Al–4 V alloys with high elastic modulus [37]. Lin et al. reported that new bone area of the Ti–6Al–4 V alloy (110 GPa) surrounded by cancellous bone decreased with time, while the new bone area of the Ti–7.5Mo alloy (65 GPa) surrounded by cancellous bone increased with time. They speculated that the less stiff Ti–7.5Mo alloy probably facilitated new bone formation in the cancellous bone area [54]. In addition to that, Johansson et al. conducted a removal torque and histomorphometric study of commercially pure Nb and Ti implants in rabbit bone, and they found that after a healing period of 3 months, a significantly higher removal torque (average 32.9 N·cm) and more bony contact (41.1%) were demonstrated for the pure Nb implants compared to the c.p. Ti ones (average 25.3 N·cm, and 37.2%), confirming the excellent bone-bonding and bone formation ability of Nb [20]. These studies suggested that the lower stiffness of the Ti–Nb alloy might be related to accelerating new bone formation compared with pure Ti, although no significant enhancement in bone formation was observed in Ti–Nb alloy possibly due to the too short *in vivo* test time. Therefore, the long-term *in vivo* bone formation assessment of the Ti–Nb alloy requires further investigation and is currently underway in the laboratory. As a consequence, *in vivo* tests clearly indicated our Ti–Nb binary alloy implant as a bioinert material, possessed the good compatibility with host bones and *in vivo* osseointegration thereby boding well to orthopedic and dental applications.

4. Conclusion

In summary, the developed Ti–45Nb binary alloy composed of β-Ti phase showed a satisfactory balance between low elastic modulus (64.3 GPa), high tensile strength (527 MPa) and high hardness (233.4 MPa). The electrochemical tests indicated that Ti–Nb alloy possessed the better corrosion resistance than pure Ti in both fluorine-free and fluorine-containing solutions. Besides, *in vitro* cytotoxicity evaluation reflected that both L929 and MG-63 cells presented a favorable attachment, proliferation, differentiation on the surface of Ti–Nb alloy. More importantly, the Ti–Nb alloy with low Young's modulus displayed any no adverse effect on new bone formation and had good bone tissue compatibility, equal to that of pure Ti. As a whole, these outcomes demonstrated the potentialities of the Ti–Nb alloy, with an elasticity similar to cortical bone and with a good cell response and osteo-compatibility, to be used as implant devices for replacing failed hard tissue.

Acknowledgment

This work was supported by the Natural Science Foundation of China (Grant 30973317) and Peking University's 985 Grant.

Appendix A. Supplementary data

Supplementary data to this article can be found online at http://dx.doi.org/10.1016/j.msec.2015.10.062.

References

[1] M. Geetha, A.K. Singh, R. Asokamani, A.K. Gogia, Ti based biomaterials, the ultimate choice for orthopaedic implants A review, Prog. Mater. Sci. 54 (2009) 397–425.
[2] D. Correa, F. Vicente, T. Donato, V. Arana-Chavez, M. Buzalaf, C.R. Grandini, The effect of the solute on the structure, selected mechanical properties, and biocompatibility of Ti–Zr system alloys for dental applications, Mater. Sci. Eng. C Mater. Biol. Appl. 34 (2014) 354–359.
[3] W.C. Head, D.J. Bauk, R.H. Emerson Jr., Titanium as the material of choice for cementless femoral components in total hip arthroplasty, Clin. Orthop. Relat. Res. 311 (1995) 85–90.
[4] C. Correa, A. Gil-Santos, J. Porro, M. Díaz, J. Ocaña, Eigenstrain simulation of residual stresses induced by laser shock processing in a Ti6Al4V hip replacement, Mater. Des. 79 (2015) 106–114.
[5] K. Miura, N. Yamada, S. Hanada, T.-K. Jung, E. Itoi, The bone tissue compatibility of a new Ti–Nb–Sn alloy with a low Young's modulus, Acta Biomater. 7 (2011) 2320–2326.
[6] M. González, J. Peña, F. Gil, J. Manero, Low modulus Ti–Nb–Hf alloy for biomedical applications, Mater. Sci. Eng. C Mater. Biol. Appl. 42 (2014) 691–695.
[7] A. Glassman, J. Bobyn, M. Tanzer, New femoral designs: do they influence stress shielding? Clin. Orthop. Relat. Res. 453 (2006) 64–74.
[8] J. Duyck, K. Vandamme, L. Geris, H. Van Oosterwyck, M. De Cooman, J. Vandersloten, R. Puers, I. Naert, The influence of micro-motion on the tissue differentiation around

immediately loaded cylindrical turned titanium implants, Arch. Oral Biol. 51 (2006) 1–9.
[9] M. Niinomi, Recent metallic materials for biomedical applications, Metall. Mater. Trans. A 33 (2002) 477–486.
[10] E. Eisenbarth, D. Velten, M. Müller, R. Thull, J. Breme, Biocompatibility of β-stabilizing elements of titanium alloys, Biomaterials 25 (2004) 5705–5713.
[11] P.R. Walker, J. LeBlanc, M. Sikorska, Effects of aluminum and other cations on the structure of brain and liver chromatin, Biochemistry 28 (1989) 3911–3915.
[12] E.D. Spoerke, N.G. Murray, H. Li, L.C. Brinson, D.C. Dunand, S.I. Stupp, Titanium with aligned, elongated pores for orthopedic tissue engineering applications, J. Biomed. Mater. Res. A 84 (2008) 402–412.
[13] D.N.A. Shri, K. Tsuchiya, A. Yamamoto, Cytocompatibility evaluation and surface characterization of TiNi deformed by high-pressure torsion, Mater. Sci. Eng. C Mater. Biol. Appl. 43 (2014) 411–417.
[14] Y. Okazaki, S. Rao, T. Tateishi, Y. Ito, Cytocompatibility of various metal and development of new titanium alloys for medical implants, Mater. Sci. Eng. A Struct. Mater. 243 (1998) 250–256.
[15] J. Xu, X.-J. Weng, X. Wang, J.-Z. Huang, C. Zhang, H. Muhammad, X. Ma, Q.-D. Liao, Potential use of porous titanium–niobium alloy in orthopedic implants: preparation and experimental study of its biocompatibility in vitro, PLoS One 8 (2013), e79289.
[16] K. Rajamallu, M.K. Niranjan, S.R. Dey, First principles theoretical investigations of low Young's modulus beta Ti–Nb and Ti–Nb–Zr alloys compositions for biomedical applications, Mater. Sci. Eng. C Mater. Biol. Appl. 50 (2015) 52–58.
[17] S. Miyazaki, H. Kim, H. Hosoda, Development and characterization of Ni-free Ti-base shape memory and superelastic alloys, Mater. Sci. Eng. A Struct. Mater. 438 (2006) 18–24.
[18] P.F. Gostin, A. Helth, A. Voss, R. Sueptitz, M. Calin, J. Eckert, A. Gebert, Surface treatment, corrosion behavior, and apatite-forming ability of Ti–45Nb implant alloy, J. Biomed. Mater. Res. B Appl. Biomater. 101 (2013) 269–278.
[19] H. Matsuno, A. Yokoyama, F. Watari, M. Uo, T. Kawasaki, Biocompatibility and osteogenesis of refractory metal implants, titanium, hafnium, niobium, tantalum and rhenium, Biomaterials 22 (2001) 1253–1262.
[20] C. Johansson, T. Albrektsson, A removal torque and histomorphometric study of commercially pure niobium and titanium implants in rabbit bone, Clin. Oral Implants Res. 2 (1991) 24–29.
[21] E. Eisenbarth, D. Velten, M. Müller, R. Thull, J. Breme, Nanostructured niobium oxide coatings influence osteoblast adhesion, J. Biomed. Mater. Res. A 79 (2006) 166–175.
[22] M. Kushwaha, X. Pan, J.A. Holloway, I.L. Denry, Differentiation of human mesenchymal stem cells on niobium-doped fluorapatite glass-ceramics, Dent. Mater. 28 (2012) 252–260.
[23] Y. Bai, Y. Wang, Y. Cheng, F. Deng, Y. Zheng, S. Wei, Comparative study on the corrosion behavior of Ti–Nb and TMA alloys for dental application in various artificial solutions, Mater. Sci. Eng. C Mater. Biol. Appl. 31 (2011) 702–711.
[24] K. Qiu, Y. Liu, F. Zhou, B. Wang, L. Li, Y. Zheng, Y. Liu, Microstructure, mechanical properties, castability and in vitro biocompatibility of Ti–Bi alloys developed for dental applications, Acta Biomater. 15 (2015) 254–265.
[25] S. He, P. Zhou, L. Wang, X. Xiong, Y. Zhang, Y. Deng, S. Wei, Antibiotic-decorated titanium with enhanced antibacterial activity through adhesive polydopamine for dental/bone implant, J. R. Soc. Interface 11 (2014) 20140169.
[26] Z. Yao, Y. Ivanisenko, T. Diemant, A. Caron, A. Chuvilin, J. Jiang, R. Valiev, M. Qi, H.-J. Fecht, Synthesis and properties of hydroxyapatite-containing porous titania coating on ultrafine-grained titanium by micro-arc oxidation, Acta Biomater. 6 (2010) 2816–2825.
[27] I. Milošev, T. Kosec, H.-H. Strehblow, XPS and EIS study of the passive film formed on orthopaedic Ti–6Al–7Nb alloy in Hank's physiological solution, Electrochim. Acta 53 (2008) 3547–3558.
[28] H.H. Huang, Effect of chemical composition on the corrosion behavior of Ni–Cr–Mo dental casting alloys, J. Biomed. Mater. Res. 60 (2002) 458–465.
[29] M. Garcıa-Alonso, L. Saldana, G. Valles, J.L. González-Carrasco, J. Gonzalez-Cabrero, M. Martınez, E. Gil-Garay, L. Munuera, In vitro corrosion behaviour and osteoblast response of thermally oxidised Ti6Al4V alloy, Biomaterials 24 (2003) 19–26.
[30] L. Shapira, A. Klinger, A. Tadir, A. Wilensky, A. Halabi, Effect of a niobium-containing titanium alloy on osteoblast behavior in culture, Clin. Oral Implants. Res. 20 (2009) 578–582.
[31] A. Cremasco, W.R. Osorio, C.M. Freire, A. Garcia, R. Caram, Electrochemical corrosion behavior of a Ti–35Nb alloy for medical prostheses, Electrochim. Acta 53 (2008) 4867–4874.
[32] D.Q. Martins, W.R. Osório, M.E. Souza, R. Caram, A. Garcia, Effects of Zr content on microstructure and corrosion resistance of Ti–30Nb–Zr casting alloys for biomedical applications, Electrochim. Acta 53 (2008) 2809–2817.
[33] Y. Zhan, C. Li, W. Jiang, β-type Ti–10Mo–1.25Si–xZr biomaterials for applications in hard tissue replacements, Mater. Sci. Eng. C Mater. Biol. Appl. 32 (2012) 1664–1668.
[34] W. Yuan, S.K. Panigrahi, J.Q. Su, R.S. Mishra, Influence of grain size and texture on Hall–Petch relationship for a magnesium alloy, Scr. Mater. 65 (2011) 994–997.
[35] E.O. Hall, The deformation and ageing of mild steel: III discussion of results, Phys. Soc. B 643 (1951) 747–752.
[36] D. Raabe, B. Sander, M. Friák, D. Ma, J. Neugebauer, Theory-guided bottom-up design of β-titanium alloys as biomaterials based on first principles calculations: theory and experiments, Acta Mater. 55 (2007) 4475–4487.
[37] M. Niinomi, T. Hattori, K. Morikawa, T. Kasuga, A. Suzuki, H. Fukui, S. Niwa, Development of low rigidity beta-type titanium alloy for biomedical applications, Mater. Trans. 43 (2002) 2970–2977.
[38] P. Vanysek, Electrochemical Series, Handbook of Chemistry and Physics, 88, 1998.
[39] B. Zhang, Y. Zheng, Y. Liu, Effect of Ag on the corrosion behavior of Ti–Ag alloys in artificial saliva solutions, Dent. Mater. 25 (2009) 672–677.
[40] M. Nakagawa, Y. Matono, S. Matsuya, K. Udoh, K. Ishikawa, The effect of Pt and Pd alloying additions on the corrosion behavior of titanium in fluoride-containing environments, Biomaterials 26 (2005) 2239–2246.
[41] M. Nakagawa, S. Matsuya, K. Udoh, Corrosion behavior of pure titanium and titanium alloys in fluoride-containing solutions, Dent. Mater. J. 20 (2001) 305–314.
[42] N. Ibriş, J.C.M. Rosca, EIS study of Ti and its alloys in biological media, J. Electroanal. Chem. 526 (2002) 53–62.
[43] S.L.d. Assis, S. Wolynec, I. Costa, Corrosion characterization of titanium alloys by electrochemical techniques, Electrochim. Acta 51 (2006) 1815–1819.
[44] H.-H. Huang, Effect of fluoride and albumin concentration on the corrosion behavior of Ti–6Al–4V alloy, Biomaterials 24 (2003) 275–282.
[45] R. Godley, D. Starosvetsky, I. Gotman, Corrosion behavior of a low modulus β-Ti–45%Nb alloy for use in medical implants, J. Mater. Sci. Mater. Med. 17 (2006) 63–67.
[46] T. Ahmed, H.J. Rack, Alloy of titanium, zirconium, niobium and tantalum for prosthetics, Google Patents, 1999.
[47] M.J. Kraay, H.L. Freese, Titanium, niobium, zirconium, and tantalum for medical and surgical applications, ASTM International, 2006.
[48] Y. Deng, Y. Sun, X. Chen, P. Zhu, S. Wei, Biomimetic synthesis and biocompatibility evaluation of carbonated apatites template-mediated by heparin, Mater. Sci. Eng. C Mater. Biol. Appl. 33 (2013) 2905–2913.
[49] J. Hong, J. Andersson, K.N. Ekdahl, G. Elgue, N. Axén, R. Larsson, B. Nilsson, Titanium is a highly thrombogenic biomaterial: possible implications for osteogenesis, Thromb. Haemost. 82 (1999) 58–64.
[50] S. Fujibayashi, M. Neo, H.-M. Kim, T. Kokubo, T. Nakamura, Osteoinduction of porous bioactive titanium metal, Biomaterials 25 (2004) 443–450.
[51] F. Nie, Y. Zheng, S. Wei, D. Wang, Z. Yu, G. Salimgareeva, A. Polyakov, R. Valiev, In vitro and in vivo studies on nanocrystalline Ti fabricated by equal channel angular pressing with microcrystalline cp Ti as control, J. Biomed. Mater. Res. A 101 (2013) 1694–1707.
[52] X. Hu, H. Shen, K. Shuai, E. Zhang, Y. Bai, Y. Cheng, X. Xiong, S. Wang, J. Fang, S. Wei, Surface bioactivity modification of titanium by CO_2 plasma treatment and induction of hydroxyapatite: in vitro and in vivo studies, Appl. Surf. Sci. 257 (2011) 1813–1823.
[53] H.M. Wong, S. Wu, P.K. Chu, S.H. Cheng, K.D. Luk, K.M. Cheung, K.W. Yeung, Low-modulus Mg/PCL hybrid bone substitute for osteoporotic fracture fixation, Biomaterials 34 (2013) 7016–7032.
[54] D.-J. Lin, C.-C. Chuang, J.-H.C. Lin, J.-W. Lee, C.-P. Ju, H.-S. Yin, Bone formation at the surface of low modulus Ti–7.5 Mo implants in rabbit femur, Biomaterials 28 (2007) 2582–2589.
[55] S.J. Li, M. Niinomi, T. Akahori, T. Kasuga, R. Yang, Y.L. Hao, Fatigue characteristics of bioactive glass-ceramic-coated Ti–29Nb–13Ta–4.6Zr for biomedical application, Biomaterials 25 (2004) 3369–3378.
[56] M. Long, H.J. Rack, Titanium alloys in total joint replacement — a materials science perspective, Biomaterials 19 (1998) 1621–1639.
[57] M. Niinomi, Mechanical properties of biomedical titanium alloys, Mater. Sci. Eng. A Struct. Mater. 243 (1998) 231–236.